

V. KOCHERGIN^{1,✉}
M. CHRISTOPHERSEN¹
H. FÖLL²

Effective medium approach for calculations of optical anisotropy in porous materials

¹ Lake Shore Cryotronics, Inc., Columbus, OH 43082, USA

² Materials Science, Faculty of Engineering, University of Kiel, Kaiserstr. 2, 24143 Kiel, Germany

Received: 22 May 2004/Revised version: 21 June 2004
Published online: 22 July 2004 • © Springer-Verlag 2004

ABSTRACT We report on a generalized approach for the calculation of optical properties of various porous semiconductors. The presented methodology provides a simple method for predicting the type and value of optical anisotropy in different materials. Specifically, the cases of electrochemically etched mesoporous Si on (110)-oriented substrate and electrochemically-etched porous InP and GaAs materials on (100) substrates are considered. The optical anisotropy of mesoporous Si is explained and the dependence of the optical birefringence of this material on various material parameters is obtained. The optical anisotropy of porous InP and GaAs with crystallographic pores is predicted based on the presented model.

PACS 78.20.-e; 78.20.Bh; 78.20.Ci; 78.20.Fm; 78.30.Fs; 78.55.Mb

1 Introduction

Engineering the optical properties of a given material by suitable modifications of its structure is a very attractive area of science and technology. Porous semiconductor materials (see, for example [1] and references therein) are important cases of such structured “metamaterials”. Semiconductors are usually turned porous by electrochemical (or photoelectrochemical) etching of the nonporous semiconductor substrates in some suitable electrolytes. To date, it has been shown that many types of semiconductors can be made in a porous form by this method. The most popular example is porous silicon, which allows the tailoring of the pore geometry from micropores (pore diameters below 2 nm; often referred to as “nanopores”), via mesopores (pore diameters between 2–50 nm) to macropores (pore diameters above 50 nm). Electrochemically etched pores have also been obtained in Ge and III-V compound semiconductors, e.g., InP, GaP, GaAs, GaN; and porous layers with many kinds of morphologies could be demonstrated [1]. The usefulness of such materials for various optical components was already outlined in [2–5]. In most cases the research has been devoted to the isotropic properties of porous semiconductors. However, recently it has been shown [6–9] that mesoporous silicon obtained from a (110) oriented substrate offers optical anisotropy properties that may be of practical importance. A remarkable result

is that in the infrared spectral range such a metamaterial offers larger values of optical birefringence than that of any commonly known natural material. Further, the combination of the value of the birefringence in the mid-to far infrared range with the transparency of these materials at the mentioned wavelengths makes these findings even more attractive for possible applications and theoretical studies.

In this paper we present a method, which provides answers to the following questions: What other porous materials can offer optical anisotropy? What kind of optical anisotropy can be expected from different porous materials? How can this anisotropy be controlled by material parameters (such as the porosity of materials, crystal orientation of the substrate, etc.)? In addition, our theoretical method could help to develop a more direct understanding of the optical effects, which is clearly lacking so far.

A method is presented for calculating the effective dielectric constants and refractive indices of different porous materials. We apply this method to several materials, already successfully fabricated by an electrochemical etching process of different semiconductors. Previously [5–7], the generalized Bruggeman method [10] was used for calculations of the optical effects in these materials. This method, while providing fair estimates for mesoporous (110)-oriented Si, is not applicable for more complex structures, employing e.g., multiple pore lattices, or for materials containing pores with noncircular cross sections. Moreover, even for the case of mesoporous silicon, which consists of a network of pores with circular cross sections growing in some preferential directions, the generalized Bruggeman method was not sufficient to provide a full and correct explanation for some of the observed effects. Looyenga formulation [26] was also applied to calculations of effective dielectric constants of porous silicon [27], however, this method is not applicable to the case of anisotropic medium. The method presented here has the capability to analyze such structures. The porous semiconductor medium is treated as macroscopically homogeneous and is assigned a dielectric permittivity tensor. Effective dielectric permittivity tensor elements depend on the dielectric constant of the semiconductor host, the dielectric constants of pore-filling materials, the pore shape, orientation and filling fraction (porosity).

2 Effective permittivity tensor calculations

In order to implement the effective medium approximation, several assumptions have to be made, which also

✉ Fax: +1-614/818-1607, E-mail: vkochergin@lakeshore.com

indicate the limitations of the model presented here. First, pores are represented by “air voids”; e.g., by air-filled cavities with elliptical shapes; cf. Fig. 1. Second, it is assumed that these air voids are uniformly and randomly distributed in the semiconductor material such that the air voids belonging to one of M lattice subsets have their axes essentially parallel to each other. Third, it is assumed that the bulk semiconductor material is isotropic and has a relative dielectric permittivity ε_B . Next, it is assumed that neighboring pores or air holes, respectively, affect each other only through the depolarization factor. This is a strong assumption that limits the validity of the method to relatively small porosities. It should be noted, however, that while this latest assumption is not strictly correct for some porous semiconductor materials, the accuracy of the approximation presented here is still good enough for a basic understanding of the optical effects taking place in such materials. Finally, we also assume that the wavelength of the electromagnetic wave considerably exceeds the cross sectional dimensions of the pores.

An electromagnetic wave with the electric field vector \mathbf{E} gives rise to a displacement vector \mathbf{D} in the porous semiconductor material, given by

$$\mathbf{D} = \varepsilon_B \mathbf{E} + \mathbf{P} \quad (1)$$

where \mathbf{P} is the effective polarization of all the particles (a pore can always be thought of as a particle in the form of an air void in semiconductor crystal) in a unit volume. With the assumptions listed above, the porous semiconductor effective dielectric permittivity tensor

$$\hat{\varepsilon}^{(\text{eff})} = \begin{pmatrix} \varepsilon_{xx}^{(\text{eff})} & \varepsilon_{xy}^{(\text{eff})} & \varepsilon_{xz}^{(\text{eff})} \\ \varepsilon_{yx}^{(\text{eff})} & \varepsilon_{yy}^{(\text{eff})} & \varepsilon_{yz}^{(\text{eff})} \\ \varepsilon_{zx}^{(\text{eff})} & \varepsilon_{zy}^{(\text{eff})} & \varepsilon_{zz}^{(\text{eff})} \end{pmatrix}$$

can be defined as follows:

$$\mathbf{D} = \hat{\varepsilon}^{(\text{eff})} \mathbf{E} \quad (2)$$

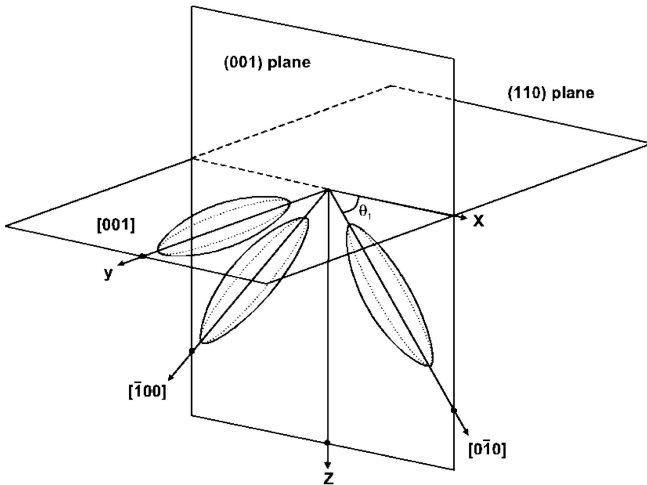


FIGURE 1 Pore structure of the mesoporous silicon grown on (110)-oriented substrate. Orientations of three major pore lattice subsets are shown

From (1) and (2) it follows:

$$\hat{\varepsilon}^{(\text{eff})} \mathbf{E} = \varepsilon_B \mathbf{E} + \mathbf{P} \quad (3)$$

Within the assumptions from above, the porous semiconductor material can be considered as an assembly of M electromagnetically separated pore lattice subsets. Hence, the polarization of the porous layer is equal to the vector sum of the polarizations of each lattice subset considered separately, or $\mathbf{P} = \sum_{i=1}^M \mathbf{P}^{(i)}$, where $\mathbf{P}^{(i)}$ is the polarization of the i th lattice subset. In this case (3) can be rewritten as:

$$\hat{\varepsilon}^{(\text{eff})} \mathbf{E} = \varepsilon_B \mathbf{E} + \sum_{i=1}^M \mathbf{P}^{(i)} \quad (3a)$$

The polarization of each pore is assumed to be a linear isotropic function of the local electric field of the electromagnetic wave, hence:

$$\mathbf{P}^{(i)} = N^{(i)} \alpha^{(i)} \mathbf{E}_L^{(i)} \quad (4)$$

$N^{(i)}$ is the density of the pores of the i th lattice subset of porous semiconductor layer, $\alpha^{(i)}$ is the polarizability of a pore in the i th lattice subset, and $\mathbf{E}_L^{(i)}$ is the local electric field as “seen” by each pore of the i th lattice subset.

The local field $\mathbf{E}_L^{(i)}$ is given by Yaghjian [11] for arbitrary shaped inclusions as

$$\mathbf{E}_L^{(i)} = \mathbf{E} + \frac{\hat{L}^{(i)} \cdot \mathbf{P}^{(i)}}{\varepsilon_B} \quad (5)$$

Where $\hat{L}^{(i)}$ is the depolarization factor that depends on the shape of the pore; it is a tensor of second rank. Under the assumptions made in the beginning of this section, the polarizability of each pore is a tensor that is always diagonalizable in a coordinate system, in which one axis coincides with the pore growth direction, i.e.,

$$\hat{\alpha}^{(i)} = \begin{pmatrix} \alpha_{1,1}^{(i)} & 0 & 0 \\ 0 & \alpha_{2,2}^{(i)} & 0 \\ 0 & 0 & \alpha_{3,3}^{(i)} \end{pmatrix}.$$

The polarization of the i th lattice subset in the coordinate system associated with said lattice subset then is

$$\tilde{\mathbf{P}}^{(i)} = \varepsilon_B \hat{M}^{(i)} \tilde{\mathbf{E}}^{(i)}$$

where

$$\hat{M}_{j,j}^{(i)} = \frac{N^{(i)} \alpha_{j,j}^{(i)}}{\varepsilon_B - L_{j,j} N^{(i)} \alpha_{j,j}^{(i)}}, \quad j = 1, 2, 3;$$

$$\text{and } \hat{M}_{j,k}^{(i)} = 0, \text{ if } j \neq k.$$

where $\tilde{\mathbf{E}}^{(i)}$ is the electric field of the electromagnetic wave in the coordinate system associated with the i th lattice subset. If the coordinate transformation matrix is introduced between the reference coordinate system (which can be associated with the crystallographic axes of the semiconductor host or anything else) and the coordinate system of i th lattice subset

$$\hat{A}^{(i)} = \begin{pmatrix} \cos \psi^{(i)} \cos \varphi^{(i)} - \cos \vartheta^{(i)} \sin \psi^{(i)} \sin \varphi^{(i)} & -\sin \psi^{(i)} \cos \varphi^{(i)} - \cos \vartheta^{(i)} \cos \psi^{(i)} \sin \varphi^{(i)} & \sin \vartheta^{(i)} \sin \varphi^{(i)} \\ \cos \psi^{(i)} \sin \varphi^{(i)} + \cos \vartheta^{(i)} \sin \psi^{(i)} \cos \varphi^{(i)} & -\sin \psi^{(i)} \sin \varphi^{(i)} + \cos \vartheta^{(i)} \cos \psi^{(i)} \cos \varphi^{(i)} & -\sin \vartheta^{(i)} \cos \varphi^{(i)} \\ \sin \vartheta^{(i)} \sin \psi^{(i)} & \sin \vartheta^{(i)} \cos \psi^{(i)} & \cos \vartheta^{(i)} \end{pmatrix}$$

where φ , ψ and θ are Euler angles, the relations $\tilde{\mathbf{E}}^{(i)} = \hat{A}^{(i)-1} \mathbf{E}$ and $\mathbf{P}^{(i)} = \hat{A}^{(i)} \tilde{\mathbf{P}}^{(i)}$ hold where \mathbf{E} and $\mathbf{P}^{(i)}$ are in the main coordinate system. Hence

$$\mathbf{P}^{(i)} = \varepsilon_{\text{InP}} \hat{A}^{(i)} \hat{M}^{(i)} \hat{A}^{(i)-1} \mathbf{E} \quad (6)$$

By substituting (6) into (3a) the effective dielectric permittivity tensor of the porous semiconductor layer is obtained as

$$\hat{\varepsilon}^{(\text{eff})} = \varepsilon_{\text{B}} \left[\hat{I} + \sum_{i=1}^M \hat{A}^{(i)} \hat{M}^{(i)} \hat{A}^{(i)-1} \right] \quad (7)$$

where $\hat{I}_{i,j} = \delta_{i,j}$.

The polarizability tensor $\hat{\alpha}$ and, in principle, the depolarization tensor \hat{L} of individual pores, need to be calculated numerically for the particular pore shape. In [12] the internal field approach combined with finite element method (FEM) has been implemented to find the polarizability tensor elements for circular, square, rectangular and triangular shape of the inclusions and here we will follow this approach.

According to the assumptions listed in the beginning of this section, the pore cross section is assumed to be much less than the wavelength of electromagnetic wave (quasi-static approximation). The internal field approach, in which the polarizability is obtained by determining the internal field of the pore, is used so the dipole moment \mathbf{d} of the air-filled pore in semiconductor material is calculated as

$$\mathbf{d} = \int_V (1 - \varepsilon_{\text{B}}) \mathbf{E} dV \quad (8)$$

and the integration is carried out only within the volume of the pore.

From another point of view, the dipole moment \mathbf{d} is defined as the product of the polarizability α and the local field \mathbf{E}_{L} . Since we assumed that the pores are electromagnetically separate, the approximation of a single pore in an infinite medium is accurate enough and, by using the results presented in [13], the dipole moment can be written as:

$$\mathbf{d} = (1 - \varepsilon_{\text{B}}) V \frac{\int_V \mathbf{E}_{\text{INT}} dV}{V} \quad (9)$$

where the internal electric field is integrated within the pore. In the dipole approximation, the electric field vector in the pore has x -, y -, z -components, but its integral over the volume of the pore will have only a component for symmetric pores aligned with respect to the electric field. Let's define β as integral of the internal electric field over the pore volume divided by said volume and the external field:

$$\beta_i = \frac{\int_V (\mathbf{E}_{\text{INT}} \cdot \mathbf{n}_i) dv}{V \cdot |\mathbf{E}_{\text{EXT}}|},$$

where \mathbf{n}_i is a unit vector collinear to i th coordinate axis direction. In the case of electric field alignment along the Cartesian direction j , the dipole moment can be written as:

$$d_j = (1 - \varepsilon_{\text{B}}) V \beta_j \mathbf{E}_{\text{EXT},j} \quad (10)$$

The integral β is thus independent on both pore volume and the external electric field of the electromagnetic wave. It can be determined either numerically or analytically. Replacing α_i in (7) by $(1 - \varepsilon_{\text{B}}) V \beta_i$, the final expression of the dielectric permittivity tensor of porous semiconductor material will be

$$\hat{\varepsilon}^{(\text{eff})} = \varepsilon_{\text{B}} \left[\hat{I} + \sum_{i=1}^M \hat{A}^{(i)} \begin{pmatrix} \frac{f_i(1-\varepsilon_{\text{B}})\beta_1^{(i)}}{\varepsilon_{\text{B}}-L_{11}f(1-\varepsilon_{\text{B}})\beta_1^{(i)}} & 0 & 0 \\ 0 & \frac{f_i(1-\varepsilon_{\text{B}})\beta_2^{(i)}}{\varepsilon_{\text{B}}-L_{22}f_i(1-\varepsilon_{\text{B}})\beta_2^{(i)}} & 0 \\ 0 & 0 & \frac{f_i(1-\varepsilon_{\text{B}})\beta_3^{(i)}}{\varepsilon_{\text{B}}-L_{33}f_i(1-\varepsilon_{\text{B}})\beta_3^{(i)}} \end{pmatrix} \hat{A}^{(i)-1} \right] \quad (11)$$

where f_i is the ‘‘porosity’’ of the i th pore lattice, and $\sum_{i=1}^M f_i = p$, $0 < p < 1$, where p is the total porosity of the porous semiconductor layer.

In the next sections the formalism developed here will be applied to some relevant examples of porous semiconductor materials.

3 (110)-oriented Si containing mesopores

The method is first applied to analyze the optical effects on mesoporous Si, which can be formed by an electrochemical etching process on (otherwise unusual) (110)-oriented silicon substrates. This porous material has been obtained recently [6] and intensively investigated with regard to its optical properties (see, for example, [5–9]). Particularly, strong in-plane birefringence (i.e., optical anisotropy) of such layers has been observed for IR wavelengths. These experimental findings were the basis for several proposed photonic devices based on such a material. For example, dichroic Bragg reflectors have been realized by Diener et al. [5], while optical polarizers have been reported in [8] and [9].

The optical anisotropy of mesoporous silicon fabricated on (110)-oriented substrates has been explained in [6] by the different filling fraction of layer in different directions (i.e., anisotropic porosity). Similar arguments have been presented in [5] to explain the different values of birefringence (i.e., optical anisotropy). In particular, the difference of the porosity

in different directions ([001] and $[\bar{1}\bar{1}0]$ crystallographic directions particularly) is proportional to the etching current during mesoporous silicon formation, i.e., proportional to the overall porosity of the sample. Drawing on the formalism developed in the previous section, we follow a different approach towards a better understanding of the optical anisotropy in mesoporous Si formed on (110)-oriented substrates, which in, our opinion, matches the experimental results better than the explanation given in [5].

In order to apply our model we first need to determine the structure of the mesoporous silicon layer grown on (110) substrate. As was shown in [14], pores in mesoporous Si propagate preferentially in equivalent $\langle 100 \rangle$ crystallographic directions independently of the substrate orientation. Hence, it can be represented as a mixture of three lattice subsets of pores collinear to the crystallographic directions mentioned. However, not all $\langle 100 \rangle$ directions are equivalent; $\langle 100 \rangle$ directions more in line with the electrical field are preferred. This is certainly due to the fact that the electric field strength at the tip then is enlarged, enabling avalanche breakdown [15] and enhancing the electrochemical dissolution reaction at the pore tip.

A schematic drawing of the ellipsoids forming by some random distribution the three pore lattice subsets found in mesoporous silicon grown on (110) wafer is shown in Fig. 1. For such a material $[\bar{1}00]$ and $[0\bar{1}0]$ pore directions are equivalent since they have identical projections in the direction of the current flow. The [001] direction, however, is perpendicular to the applied current direction, since it lies in (110) crystallographic plane.

In the analyses presented, it is assumed that the pores in each lattice can be represented as distribution of ellipsoids, which are elongated in the direction of each pore lattice. Such an assumption is in agreement with extensive XRD investigations of different porous layers presented in [16]. In this case (11) takes the following form:

$$\hat{\varepsilon}^{(\text{eff})} = \varepsilon_{\text{Si}} \left[\hat{I} + \sum_{i=1}^3 \hat{A}^{(i)} \hat{M}^{(i)} \hat{A}^{(i)-1} \right] \quad (12)$$

The pore lattices collinear to the $[0\bar{1}0]$, $[\bar{1}00]$, and [001] crystallographic directions have been assigned index (1), (2), and (3); respectively. It is farther assumed that the individual pores represented by ellipsoids are of the same shape and volume, however, the filling fraction of the pores of the first and second pore lattices exceeds that of the third pore lattice due to the current flow direction, i.e., $f^{(1)} = f^{(2)}$ and $f^{(3)} < f^{(1)}$. With this assumption, depolarization factors and polarizabilities for each pore lattice are the same.

Let us introduce the local pore lattice coordinate system such that the x axis is parallel to the pore lattice direction and y axis lies in the (110) plane. The depolarization factor for the longer axis of the ellipsoid L_{11} depends on the ratio $x = c/a$ ($a > b = c$) between the axes lengths as (see [17]):

$$L_{11} = \frac{x^2}{(1-x^2)^{3/2}} \left[\text{arcth} \left(\sqrt{1-x^2} \right) - \sqrt{1-x^2} \right] \quad (13)$$

Due to the circular cross section of the pores in mesoporous Si, $L_{22} = L_{33} = (1 - L_{11})/2$ obtains.

If the reference coordinate system is introduced as shown in Fig. 1 (X -axis is directed in the $[\bar{1}\bar{1}0]$ direction and Y -axis in [001]), the coordinate transformation matrices will be as follows:

$$\hat{A}^{(1)} = \begin{pmatrix} \frac{\sqrt{2}}{2} & 0 & -\frac{\sqrt{2}}{2} \\ 0 & 1 & 0 \\ \frac{\sqrt{2}}{2} & 0 & \frac{\sqrt{2}}{2} \end{pmatrix}, \quad \hat{A}^{(2)} = \begin{pmatrix} -\frac{\sqrt{2}}{2} & 0 & \frac{\sqrt{2}}{2} \\ 0 & -1 & 0 \\ \frac{\sqrt{2}}{2} & 0 & \frac{\sqrt{2}}{2} \end{pmatrix},$$

$$\hat{A}^{(3)} = \begin{pmatrix} 0 & 1 & 0 \\ -1 & 0 & 0 \\ 0 & 0 & 1 \end{pmatrix}$$

If the porosity of the mesoporous silicon layer is p and the coefficient r is introduced to describe the ratio of filling fractions between the [001] pore lattice and other lattices, the electrical polarization matrices for each lattice will be as follows:

$$M_{1,1}^{(1)} = M_{1,1}^{(2)} = \frac{(p - pr)(1 - \varepsilon_{\text{Si}})\beta_1}{2\varepsilon_{\text{Si}} - L_{11}(p - pr)(1 - \varepsilon_{\text{Si}})\beta_1},$$

$$M_{2,2}^{(1)} = M_{2,2}^{(2)} = M_{3,3}^{(1)} = M_{3,3}^{(2)} = \frac{2(p - pr)(1 - \varepsilon_{\text{Si}})\beta_2}{4\varepsilon_{\text{Si}} - (1 - L_{11})(p - pr)(1 - \varepsilon_{\text{Si}})\beta_2},$$

$$M_{1,1}^{(3)} = \frac{pr(1 - \varepsilon_{\text{Si}})\beta_1}{\varepsilon_{\text{Si}} - L_{11}pr(1 - \varepsilon_{\text{Si}})\beta_1},$$

$$M_{2,2}^{(3)} = M_{3,3}^{(3)} = \frac{2pr(1 - \varepsilon_{\text{Si}})\beta_2}{2\varepsilon_{\text{Si}} - (1 - L_{11})pr(1 - \varepsilon_{\text{Si}})\beta_2}$$

The values of the coefficients β_1 and β_2 according to [17] are:

$$\beta_1 = \frac{\varepsilon_{\text{Si}}}{\varepsilon_{\text{Si}} - (\varepsilon_{\text{Si}} - 1)L_{11}}$$

$$\beta_2 = \frac{\varepsilon_{\text{Si}}}{\varepsilon_{\text{Si}} - (\varepsilon_{\text{Si}} - 1)L_{22}} = \frac{2\varepsilon_{\text{Si}}}{2\varepsilon_{\text{Si}} - (\varepsilon_{\text{Si}} - 1)(1 - L_{11})}$$

We now determine the dielectric properties of mesoporous silicon layer grown on (110) substrate for the following assumptions: the overall porosity is 25%, the aspect ratio of the pore ellipsoids is 0.5 (i.e., longer axis of the ellipsoid is twice longer than other two axes), the parameter r is 0.1. The refractive index of Si is assumed to be 3.5 with zero imaginary part (which is true for wavelengths exceeding the band edge of Si around 1100 nm and smaller than free carrier absorption edge). Substituting the parameters into (12) gives the following value of the dielectric permittivity tensor in the coordinate system as shown in Fig. 1:

$$\hat{\varepsilon}^{(\text{eff})} = \begin{pmatrix} 8.421 & 0 & 0 \\ 0 & 8.1 & 0 \\ 0 & 0 & 8.421 \end{pmatrix}.$$

This result based on the effective medium model presented in the previous section means that mesoporous silicon grown on (110)-substrate will be a negative uniaxial crystal with an optical axis that coincides with the $\langle 001 \rangle$ direction. The angular dependence of the numerically calculated dielectric

permittivity tensor components of such a material is given in Fig. 2. Suffice it to state that the model anisotropy type predicted by the theory presented is in complete agreement with experimental findings as reported in [6] and [5].

The optical anisotropy of such a material is well known (see, for example [18]). In such crystals for any direction of the electric field in the electromagnetic wave two eigensolutions of the secular equation exist, which are called ordinary and extraordinary waves and described by refractive indices usually denoted n_o and n_e . In the coordinate system as drawn in Fig. 1, $n_o = \sqrt{\epsilon_{xx}^{(eff)}} \equiv \sqrt{\epsilon_{zz}^{(eff)}}$, while $n_e = \sqrt{\epsilon_{yy}^{(eff)}}$. The normal surface of the electromagnetic waves in this case consists of a sphere and an ellipsoid of revolution, contained in the sphere. For any direction of light propagation in such a crystal two waves with different refractive indices exist that have two different polarization states: an ordinary wave, which always has the refractive index n_o and is polarized such that the electric field of the electromagnetic wave is in the (001) plane, and an extraordinary wave which has a refractive index as defined by:

$$\frac{1}{n_e^2(\theta)} = \frac{\cos^2 \theta}{n_o^2} + \frac{\sin^2 \theta}{n_e^2},$$

where θ is the angle between the electromagnetic wave propagation direction and the [001] crystal axis. The direction of polarization for the extraordinary electric field for the case of the plane of incidence being the (110) plane, is given by

$$\begin{pmatrix} 0 \\ \frac{\cos \theta}{n_e^2(\theta) - n_o^2} \\ \frac{\sin \theta}{n_e^2(\theta) - n_o^2} \end{pmatrix}.$$

The value $(n_o - n_e)/n_o$ of the relative optical anisotropy depends on the porosity of the sample, on the relative filling fraction of the [001] pore lattice subsets, and on the pore ellipsoid aspect ratio. The plots of these dependences are given in Fig. 3. In all of the pictures, the porosity of the sample was assumed to be 25%, the aspect ratio of the pore ellipsoids is 0.5, and the relative filling fraction of the [001] pore lattice subset is 0.1 if it is not stated otherwise. One can see that the dependence of the relative optical anisotropy of the material is linearly proportional to the porosity of the sample if both other parameters are assumed to be constant. However, it is highly likely that both parameters can change with experimental conditions that create different porosities in the material. Unfortunately, no extensive experimental investigation of the relative optical anisotropy vs. porosity of the sample is published to date. Such data, interpreted with the formalism presented here, could provide straightforward information on the changes of the morphology of the mesoporous Si layers with porosity.

In any case, based on the results following from the formalism presented in the previous section, it is safe to state that optical anisotropy in the mesoporous silicon etched on the (110)-oriented substrate is not due to the anisotropic porosity of the material, but rather due to: 1) anisotropic polarizability and depolarization factors of the pores in each pore lattice, 2) preferential ordering of the pores into three distinct lattices,

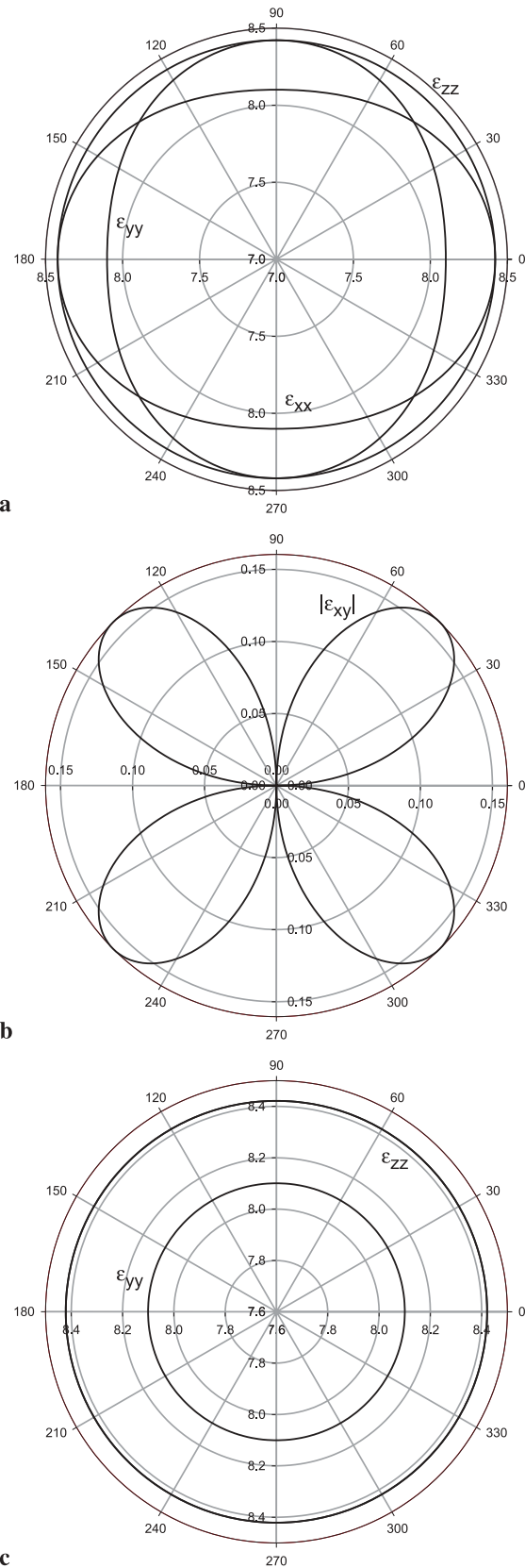


FIGURE 2 The polar plots of the elements of the dielectric permittivity tensor of mesoporous silicon grown on (110)-oriented substrate: **a** diagonal tensor elements for the case of electric field rotated in the (110) plane; **b** the only nonzero nondiagonal tensor element for the case of electric field rotated in the (110) plane, and **c** diagonal tensor elements for the case of electric field rotated in the (100) plane

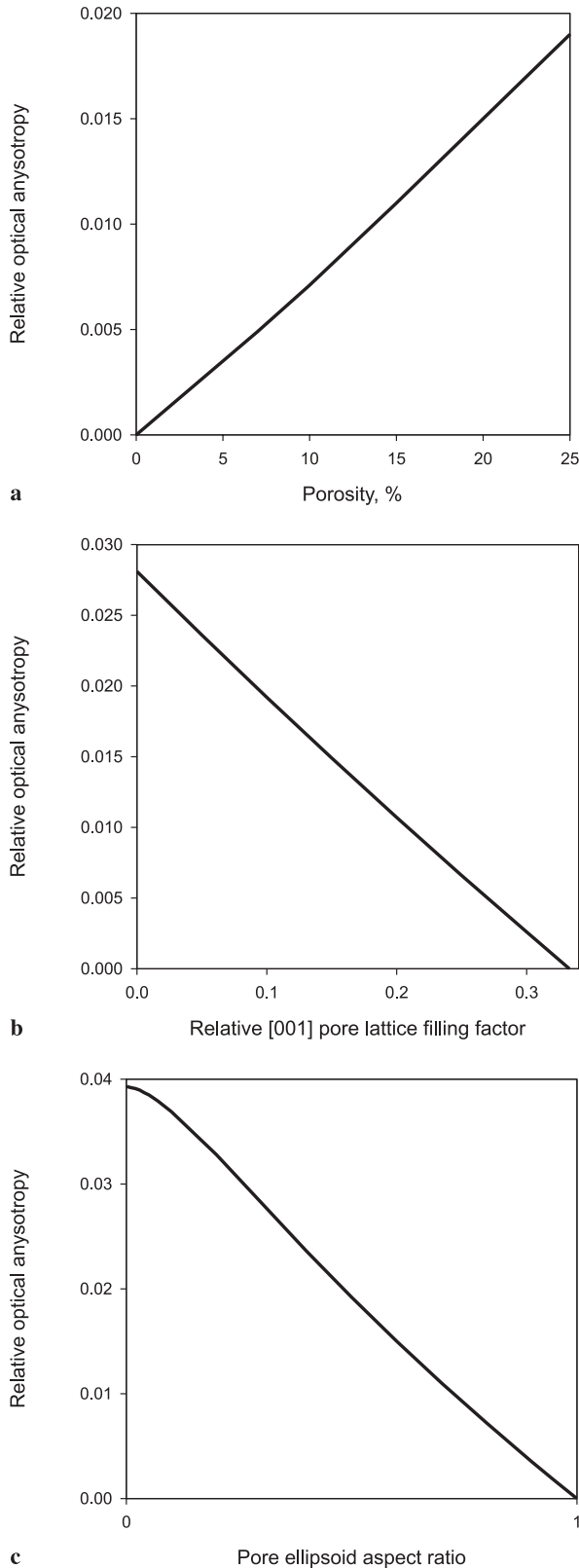


FIGURE 3 **a** Calculated dependence of the relative optical anisotropy of mesoporous silicon etched on (110) oriented substrate on the porosity of the material; **b** calculated dependence of the relative optical anisotropy of mesoporous silicon etched on (110) oriented substrate on the relative filling ratio of the [001] pore lattice of the material, and **c** calculated dependence of the relative optical anisotropy of mesoporous silicon etched on (110) oriented substrate on the pore ellipsoid aspect ratio of the [001] pore lattice of the material

and 3) smaller filling ratio of the pores aligned into [001] lattice compared to those aligned into [100] and [010] lattices. The relative optical anisotropy of the material is expected to increase with the porosity of the material even if the relative filling fraction of the [001] pore lattice stays the same. With more experimental data available, the effective medium method theory developed here could help to bring more insights into the pore morphology. The anisotropy of the mesoporous silicon etched on differently oriented substrates can be also easily investigated with the methodology presented here.

4 (100)-oriented InP and GaAs containing crystallographic pores

Other interesting examples of porous materials are porous InP [19–21] and porous GaAs [20–22] with crystallographically oriented pores. These pores have definite crystallographic growth directions in $\langle 111 \rangle$ B for GaAs, InP, and GaP (in contrast to $\langle 100 \rangle$ and $\langle 113 \rangle$ for Si [24] and $\langle 100 \rangle$ for Ge [25]). In the $\langle 111 \rangle$ directions the zincblende lattice of the III-V compounds consists of double layers with alternating short (three bonds) and long (one bond) distances, and the layers are occupied by A-type (In, Ga) or B-type (P, As) atoms. The $\langle 111 \rangle$ B direction then runs from B to A layers along the shortest distance between A and B planes (or from B to A along the longest distance between the A and the B planes). It is important to note that A planes are generally more stable against electrochemical dissolution than B planes. The so-called $\langle 111 \rangle$ A directions can be represented as $-Ga \equiv As-Ga \equiv As-$, while the second set ($\langle 111 \rangle$ B) can be represented as $-As \equiv Ga-As \equiv Ga-$ ($-$ means one bond) [23]. For the GaAs case, an (100)-oriented GaAs wafer has four $\langle 111 \rangle$ directions that are preferential crystallographic directions for pore growth, thus offering four directions for pore growth. If all four $\langle 111 \rangle$ B directions will be expressed depends on the nucleation conditions for the pores. Two general types of pore nucleation have been observed during the anodization: uniform and non-uniform. Non-uniform nucleation usually resulted in formation of “pore domains” on the surface of the sample. Figure 4 shows a cross section SEM micrograph and an overview of the nucleation for a domain of pores in GaAs. We focused our studies on porous domains in GaAs with all four $\langle 111 \rangle$ B directions present – see schematic drawing in Fig. 4. The SEM images of such a porous GaAs layer are shown in Fig. 4a and b. It should be noted, that the pore cross-section is in this case of triangular shape (see Fig. 4b), unlike the case of mesoporous silicon, considered in the previous section. The situation with crystallographic InP porous layer is substantially the same.

To apply the effective medium method presented here, we need to consider four pore lattices, as shown in Fig. 4c. In this case (11) takes the following form:

$$\hat{\varepsilon}^{(\text{eff})} = \varepsilon_{\text{GaAs}} \left[\hat{I} + \sum_{i=1}^4 \hat{A}^{(i)} \hat{M}^{(i)} \hat{A}^{(i)-1} \right] \quad (14)$$

Simple geometrical derivations lead to the following coordinate transformation matrices, if the reference coordinate system is introduced as shown in Fig. 4c. The X - and Y -axes are collinear to the projections of pore growth directions

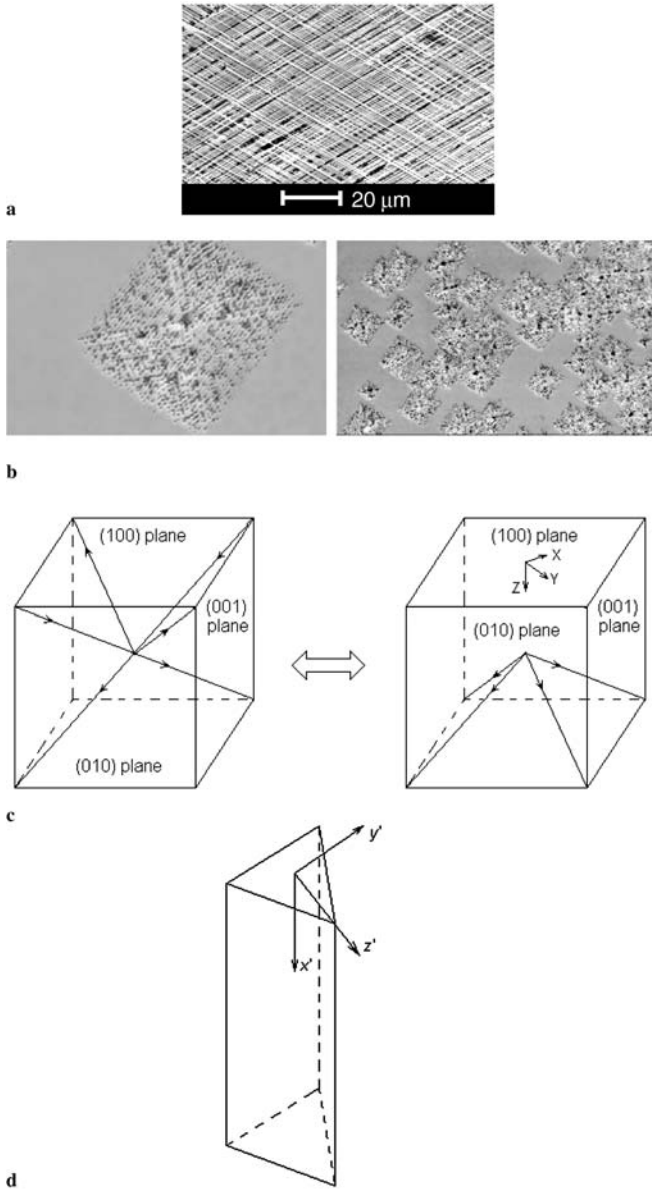


FIGURE 4 **a, b** SEM images of the porous GaAs layer with crystallographic pores; **c** the schematic drawing showing the pore lattices accounted by the model for the case of porous GaAs or InP electrochemically etched on (100) oriented substrates, and **d** the coordinate system associated with the pore lattice

($\langle 111 \rangle$ directions) on the (100) plane:

$$\hat{A}^{(1)} = \begin{pmatrix} \sqrt{\frac{2}{3}} & 0 & -\frac{1}{\sqrt{3}} \\ 0 & 1 & 0 \\ \frac{1}{\sqrt{3}} & 0 & \sqrt{\frac{2}{3}} \end{pmatrix}, \quad \hat{A}^{(2)} = \begin{pmatrix} 0 & 1 & 0 \\ -\sqrt{\frac{2}{3}} & 0 & \frac{1}{\sqrt{3}} \\ \frac{1}{\sqrt{3}} & 0 & \sqrt{\frac{2}{3}} \end{pmatrix},$$

$$\hat{A}^{(3)} = \begin{pmatrix} -\sqrt{\frac{2}{3}} & 0 & \frac{1}{\sqrt{3}} \\ 0 & -1 & 0 \\ \frac{1}{\sqrt{3}} & 0 & \sqrt{\frac{2}{3}} \end{pmatrix}, \quad \hat{A}^{(4)} = \begin{pmatrix} 0 & -1 & 0 \\ \sqrt{\frac{2}{3}} & 0 & -\frac{1}{\sqrt{3}} \\ \frac{1}{\sqrt{3}} & 0 & \sqrt{\frac{2}{3}} \end{pmatrix}$$

Let us calculate first the dielectric permittivity for the illustrative case of round pores. In this case, as in the mesoporous

silicon case considered in the previous section, $\beta_{22} = \beta_{33}$ and $L_{22} = L_{33}$. The calculations performed for the 15% porosity give the value of the dielectric permittivity tensor

$$\hat{\varepsilon}^{(\text{eff})} = \begin{pmatrix} 7.795 & 0 & 0 \\ 0 & 7.795 & 0 \\ 0 & 0 & 7.795 \end{pmatrix}.$$

It means that the porous InP or GaAs layers would be optically isotropic materials if the pores were of circular cross-section. However, as mentioned above, the pores in these materials have triangular cross sections, i.e., $\beta_{22} \neq \beta_{33}$ and $L_{22} \neq L_{33}$ (see Fig. 4d for the coordinate system associated with pore lattices).

We now need to determine the values of the L_{ii} and β_i coefficients. Unlike in the mesoporous Si case described in the previous section, the pores in InP or GaAs cannot be considered as inclusions with some aspect ratio since the pores usually extend through the whole thickness of the sample. Hence, with good accuracy (assuming that the layer of porous InP or GaAs is thick enough compared to the pore cross section, typically around 300 nm), $L_{11} = 0$ and $\beta_1 = 1$. According to [12] for equilateral triangular shape inclusions $L_{22} = 0.5$. Hence, $L_{33} = 1 - L_{22} = 0.5$ as well. In our calculations the value of β_2 was assumed to be 1.88, while $\beta_3 = 1.81$.

Numerical calculations for triangular shaped pores 15% porosity returned the following value of the dielectric permittivity tensor of InP:

$$\hat{\varepsilon}^{(\text{eff})} = \begin{pmatrix} 7.61 & 0 & 0 \\ 0 & 7.61 & 0 \\ 0 & 0 & 7.659 \end{pmatrix}$$

and the following value for GaAs:

$$\hat{\varepsilon}^{(\text{eff})} = \begin{pmatrix} 9.639 & 0 & 0 \\ 0 & 9.639 & 0 \\ 0 & 0 & 9.702 \end{pmatrix}.$$

The angular dependence of the numerically calculated dielectric permittivity tensor components of such a material is given in Fig. 5. Porous InP and GaAs with crystallographic pores thus are positive uniaxial crystals and the optical axis coincides with the [100] direction. The optical anisotropy, hence, cannot be observed at normal incidence. The refractive index of the ordinary and extraordinary beams in coordinate system as drawn in Fig. 4c (left) are $n_o = \sqrt{\varepsilon_{xx}^{(\text{eff})}} \equiv \sqrt{\varepsilon_{yy}^{(\text{eff})}}$, while $n_e = \sqrt{\varepsilon_{zz}^{(\text{eff})}}$. The normal surface of the electromagnetic waves in this case consists of an ellipsoid of revolution and a sphere contained in the ellipsoid. The value of the optical anisotropy of such materials is predicted to be far less than that of mesoporous silicon etched on (110) oriented substrate. It is predicted to be higher for GaAs, since it has a higher refractive index than InP.

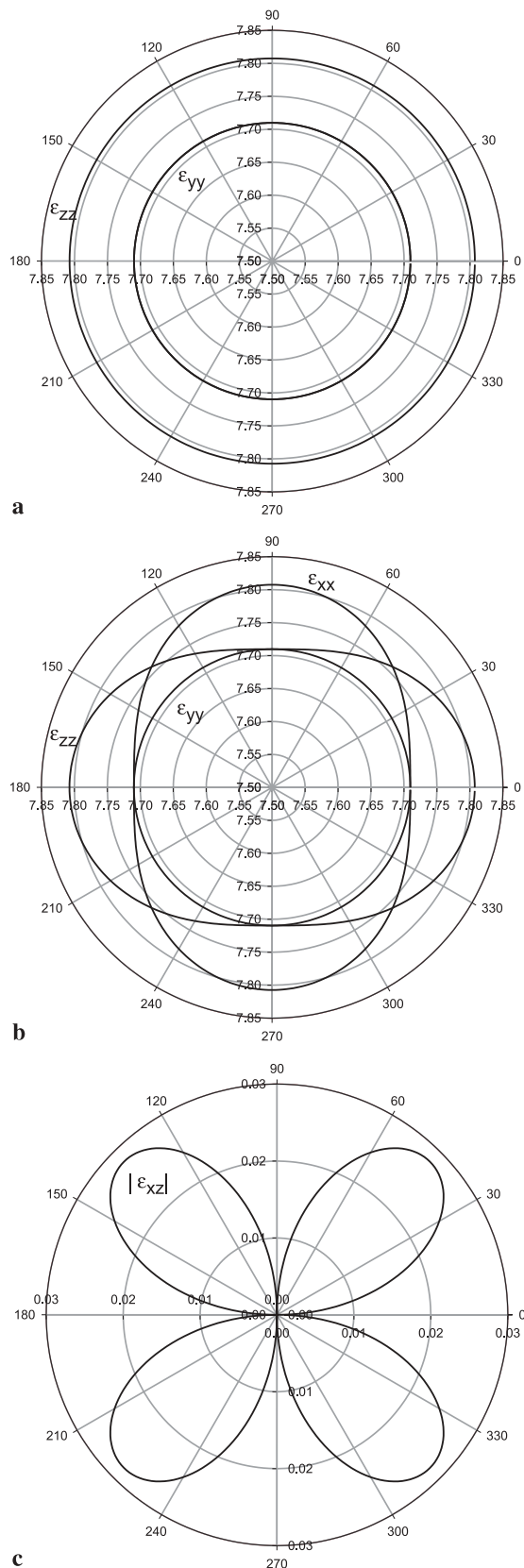


FIGURE 5 Calculated polar plots of the elements of the dielectric permittivity tensor of porous InP grown on (100)-oriented substrate: **a** diagonal tensor elements for the case of electric field rotated in the XOY (100) plane; **b** the diagonal tensor elements for the case of electric field rotated in the XOZ plane, and **c** nondiagonal tensor element for the case of electric field rotated in the XOZ plane

5 Conclusions:

The effective-medium method presented here provides a valuable and reliable tool for the quick evaluation of optical properties of various kinds of porous semiconductor materials. The methodology presented in this paper has been successfully applied to the practical cases of mesoporous silicon grown on (110)-oriented substrate and porous InP and GaAs etched on (100) oriented substrates with crystallographic pores. The results of the application of the effective medium approach to the mesoporous silicon etched on (110) oriented substrates are in complete agreement with experimental findings presented in, for example, [5, 6]. The methodology presented here helped to provide a correct understanding of the appearance of the optical anisotropy in such a material, and can provide a valuable and simple tool for the investigation of the morphology of mesoporous silicon layers when more experimental data will be available. In addition, based on the theoretical analyses of porous InP or GaAs with crystallographic pores etched on (100) wafers, an optical anisotropy is predicted, which is based not on the orientation and filling fractions of different pore lattices as in the mesoporous silicon case for (110) substrates, but rather on the triangular shape of the pores. Although the method presented was exemplary applied only for these materials, it can be easily adapted to other porous materials.

REFERENCES

- H. Föll, S. Langa, J. Carstensen, M. Christophersen, I.M. Tiginyanu: *Adv. Materials* **15**, 183 (2003)
- G. Vincent: *Appl. Phys. Lett.* **64**, 2367 (1994)
- V. Pellegrini, A. Tredicucci, C. Mazzoleni, L. Pavesi: *Phys. Rev. B* **52**, 14328 (1995)
- V. Kochergin: *Omnidirectional Optical Filters* (Kluwer Academic Publishers, Boston 2003)
- J. Diener, N. Künzner, D. Kovalev, E. Gross, V.Y. Timoshenko, G. Polisski, F. Koch: *Appl. Phys. Lett.* **78**, 3887 (2001)
- D. Kovalev, G. Polisski, J. Diener, H. Heckler, N. Künzner, V.Y. Timoshenko, F. Koch: *Appl. Phys. Lett.* **78**, 916 (2001)
- J. Diener, N. Künzner, D. Kovalev, E. Gross, F. Koch: *J. Appl. Phys.* **91**, 6704 (2002)
- J. Diener, N. Künzner, E. Gross, D. Kovalev, M. Fujii: *Opt. Lett.* **29**, 195 (2004)
- Q.H. Wu, L. De Silva, M. Arnold, I.J. Hodgkinson, E. Takeuchi: *J. Appl. Phys.* **95**, 402 (2004)
- D.A.G. Bruggeman: *Ann. Phys. (Paris)* **24**, 636 (1935)
- A.D. Yaghjian: *Proc. IEEE* **68**, 248 (1980)
- M. Maldovan, M.R. Bockstaller, E.L. Thomas, W.C. Carter: *Appl. Phys. B* **76**, 877 (2003)
- A. Shivola, I.V. Lindell: *J. Electromagnetic Waves Applic.* **3**, 37 (1989)
- A.G. Cullis, L.T. Canham, P.D.J. Calcott: *J. Appl. Phys.* **82**, 909 (1997)
- V.V. Lehmann, R. Stengl, A. Luigart: *Mater. Sci. Eng., B* **69–70**, 11 (2000)
- C. Faivre, D. Bellet: *J. Appl. Cryst.* **32**, 1134 (1999)
- L.D. Landau, E.M. Lifshits: *Electrodynamics of Continuous Media*, 2nd edn. (Butterworth-Heinemann, Oxford 1984)
- A. Yariv, P. Yeh: *Optical Waves in Crystals* (John Wiley & Sons, New York 1984)
- S. Langa, I.M. Tiginyanu, J. Carstensen, M. Christophersen, H. Föll: *J. Electrochem. Soc. Lett.* **3**, 514 (2000)
- H. Föll, J. Carstensen, S. Langa, M. Christophersen, I.M. Tiginyanu: *Phys. Stat. Sol. A* **197**, 61 (2003)
- H. Föll, S. Langa, J. Carstensen, M. Christophersen, I.M. Tiginyanu: *Adv. Mater. Rev.* **15**, 183 (2003)
- B.H. Erne, D. Vanmaekelbergh, J.J. Kelly: *J. Electrochem. Soc.* **143**, 305 (1996)

-
- 23 P.H.L. Notten, J.E.A.M. van den Meerakker, J.J. Kelly: *Etching of III-V Semiconductors: An Electrochemical Approach* (Elsevier Science Publishers Ltd., Oxford 1991)
- 24 M. Christophersen, J. Carstensen, S. Rönnebeck, C.J.W. Jäger, H. Föll: *J. Electrochem. Soc.* **148**, E-267 (2001)
- 25 S. Langa, M. Christophersen, J. Carstensen, I.M. Tiginyanu, H. Föll: *Phys. Stat. Sol. A* **195**, R4 (2003)
- 26 H. Looyenga: *Physica* **31**, 401 (1965)
- 27 J. Zettner, M. Thoenissen, T. Hierl, R. Brendel, M. Schulz: *Prog. Photovoltaics* **6**, 423 (1999)